Available online at www.sciencedirect.com
ScienceDirect
International Journal of Solids and Structures 44 (2007) 4559–4573
INTERNATIONAL JOURNAL OF SOLIDS and STRUCTURES
www.elsevier.com/locate/ijsolstr

Split singularities and the competition between crack penetration and debond at a bimaterial interface

Zhen Zhang, Zhigang Suo *

Division of Engineering and Applied Sciences, Harvard University, Cambridge, MA 02138, USA

Received 15 June 2006; received in revised form 17 November 2006
Available online 1 December 2006

Abstract

For a crack impinging upon a bimaterial interface at an angle, the singular stress field is a linear superposition of two modes, usually of unequal exponents, either a pair of complex conjugates, or two unequal real numbers. In the latter case, a stronger and a weaker singularity coexist (known as split singularities). We define a dimensionless parameter, called the local mode mixity, to characterize the proportion of the two modes at the length scale where the processes of fracture occur. We show that the weaker singularity can readily affect whether the crack will penetrate, or debond, the interface.

Keywords: Interface; Crack; Fracture; Split singularities; Local mode mixity

1. Introduction

It is well known that, for a crack in a homogeneous elastic material under the plane strain conditions, the singular stress field is a linear superposition of two modes, both having the exponent of 1/2. Despite its central importance in fracture mechanics, a crack in a homogeneous material is a particular case among many configurations of bonded wedges of dissimilar elastic materials; see Akisanya and Fleck (1997), Reedy (2000), Mohammed and Liechti (2000) and Labossiere et al. (2002) for reviews of literature. For such a configuration, the singular stress field may still consist of two modes, but usually of *unequal exponents*, either a pair of complex conjugates, or two unequal real numbers. The two exponents may degenerate to one real number for special choices of the materials and the geometry, but a perturbation in the parameters characterizing the materials and the geometry often lifts the degeneracy, leading to two unequal exponents. Thus, unequal exponents are a rule rather than an exception.

The case of complex-conjugate exponents has been extensively discussed within the context of a crack lying on a bimaterial interface (e.g., Rice, 1988). This paper will focus on the case that the two modes have unequal real exponents. That is, a stronger and a weaker singularity coexist, a situation known as the *split singularities*.

* Corresponding author. Tel.: +1 617 495 3789; fax: +1 617 496 0601.
E-mail address: suo@deas.harvard.edu (Z. Suo).

0020-7683/$ - see front matter
doi:10.1016/j.ijsolstr.2006.11.035

It is sometimes suggested that the stronger singularity should be used to formulate failure criteria. However, Liu et al. (1999) have shown that the stronger singularity may dominate only within an exceedingly small zone, and argued that both singularities can be important. Labossiere et al. (2002) have included both modes in studying fracture initiated from a bimaterial corner.

This paper aims to show the significance of the split singularities in a particular context. Fig. 1 illustrates two elastic materials bonded at an interface, and a crack impinging upon the interface at angle ω, with the edge of the crack lying on the interface. For many combinations of the materials and the impinging angle, the two modes of the singular stress field have unequal real exponents (e.g., Bogy, 1971; Ashaugh, 1975; Fenner, 1976; Chen and Wang, 1996; Li et al., 1997). The impinging crack may either penetrate across, or debond, the interface (Fig. 2), a competition that has been extensively studied (e.g., Cook and Gordon, 1964; He and Hutchinson, 1989a; Thouless et al., 1989; Gupta et al., 1992; Martinez and Gupta, 1994; Lemaitre et al., 1996; Kovar et al., 1998; Davis et al., 2000; Leguillon et al., 2000, 2001; Joyce et al., 2003; Roham et al., 2004; Parmigiani and Thouless, 2006). The effects of the split ingularities on this competition, however, have never been considered. This paper will show that the weaker singularity can readily alter the outcome of the penetration–debond competition.

2. Split singularities

To set the stage, this section describes the salient features of the singularities of a crack impinging on a bimaterial interface (Fig. 1). When both materials are elastic and isotropic, for problems of this type Dundurs (1969) has shown that the stress field depends on elastic constants through two dimensionless parameters:

$$\alpha = \frac{\mu_1(1-\nu_2) - \mu_2(1-\nu_1)}{\mu_1(1-\nu_2) + \mu_2(1-\nu_1)}, \tag{1}$$

$$\beta = \frac{1}{2}\left[\frac{\mu_1(1-2\nu_2) - \mu_2(1-2\nu_1)}{\mu_1(1-\nu_2) + \mu_2(1-\nu_1)}\right], \tag{2}$$

where μ is the shear modulus, and ν Poisson's ratio. The subscripts 1 and 2 refer to the two materials, respectively. By requiring $0 \leqslant \nu \leqslant 0.5$ and $\mu > 0$, the Dundurs parameters are confined within a parallelogram in the (α, β) plane, with vertices at $(1,0)$, $(1,0.5)$, $(-1,0)$ and $(-1,-0.5)$.

For the singular stress field around the edge of the crack, a component of the stress tensor, say $\sigma_{\theta\theta}$, takes the form of $\sigma_{\theta\theta} \sim r^{-\lambda}$. The exponent λ is a root of a transcendental equation given by Bogy (1971). The root is restricted as $0 < \mathrm{Re}(\lambda) < 1$, a restriction commonly adopted, with justifications critiqued by Hui and Ruina

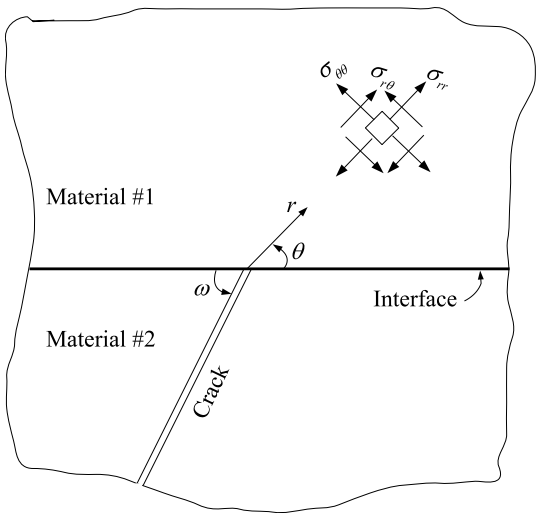

Fig. 1. Two materials, #1 and #2, occupy two half spaces and are bonded at an interface. A crack pre-exists in material #2, impinging upon the interface at angle ω. The edge of the crack lies on the interface, and coincides with the z-axis of a polar coordinate system (r, θ, z).

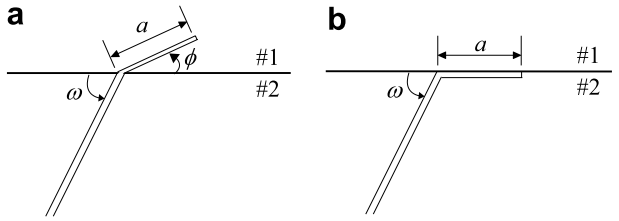

Fig. 2. After a primary crack in material #2 hits the interface, the crack may go on to either (a) penetrate into material #1, or (b) debond the interface. The angle of penetration, ϕ, may be determined by the criterion that the penetrating crack is purely mode I. The length of the small cracks, a, may represent the size of flaws in material #1 and on the interface.

(1995) and Dunn et al. (2001). Depending on the Dundurs parameters α and β, as well as on the impinging angle ω, the solution of the exponent can be either two real numbers λ_1 and λ_2, or a pair of complex conjugates $\lambda_{1,2} = \xi \pm i\varepsilon$, where $\mathrm{i} = \sqrt{-1}$.

For the impinging angle $\omega = 45°$, for example, Fig. 3 plots the contours of the exponents on the (α, β) plane. The parallelogram is divided into four regions by dark curves meeting at the center $\alpha = \beta = 0$. In the upper-left and lower-right regions, the exponents are real and unequal. The contours of larger exponent (λ_1) are labeled horizontally, and the contours of the smaller exponent (λ_2) are labeled vertically. When $\alpha < 0$, material #2 is stiffer than material #1, and $\lambda_1 > \lambda_2 \geqslant 0.5$. When $\alpha > 0$, material #1 is stiffer than material #2, and $\lambda_2 < \lambda_1 \leqslant 0.5$. In the upper-right and lower-left regions, the exponents are a pair of complex conjugates, $\lambda_{1,2} = \xi \pm i\varepsilon$. The contours of the real part ξ are solid lines, and are strongly α-dependent. The contours of the imaginary part ε are dashed lines, and are strongly β-dependent. These four regions are separated by the four boundaries (i.e., the dark curves). At each point on the boundaries, the two exponents degenerate to one number: when the point is approached from a region of real exponents, the two exponents become identical; when the point is approached from a region of complex-conjugate exponents, the imaginary part vanishes. At $\alpha = \beta = 0$, the two materials have the same elastic constants, and the two exponents are degenerate, $\lambda_1 = \lambda_2 = 0.5$, corresponding to the familiar two modes at the edge of a crack in a homogeneous material.

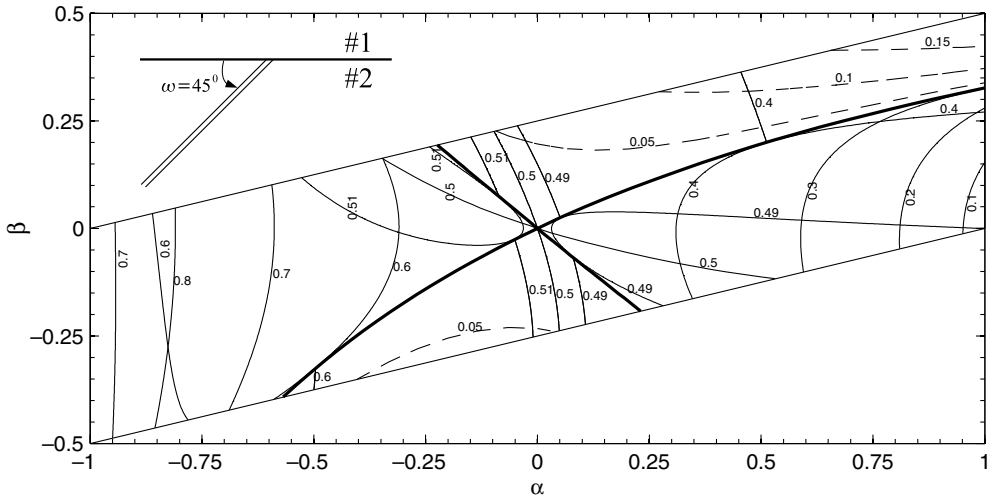

Fig. 3. Contours of the exponents of the singular stress field around the tip of a crack impinging on the interface at angle $\omega = 45°$, plotted on the plane of the Dundurs parameters (α, β), is restricted in the parallelogram. The parallelogram is divided into four regions with the boundaries denoted by the dark curves. In the upper-left and lower-right regions, the exponents are two unequal real numbers, with the larger exponent λ_1 labeled horizontally, and the smaller exponent λ_2 labeled vertically. In the upper-right and lower-left regions, the exponents are a pair of complex conjugates, with the real part ξ plotted as solid lines, and the imaginary part ε as dashed lines. On the boundaries (the dark curves), the exponents of the two modes degenerate to one number.

These contours change as the impinging angle ω varies. As a limiting case, first studied by Williams (1959), when the crack lies on the interface ($\omega = 0$), the exponents are a pair of complex conjugates

$$\lambda_{1,2} = \frac{1}{2} \pm i\frac{1}{2\pi}\ln\frac{1-\beta}{1+\beta}. \tag{3}$$

In this case, the regions of complex conjugates expand to the whole (α, β) plane, except for the line $\beta = 0$, where $\lambda_1 = \lambda_2 = 0.5$. The interfacial crack has been extensively studied; see reviews by Rice (1988) and by Hutchinson and Suo (1992).

As another limiting case, first studied by Zak and Williams (1963), when the crack is perpendicular to the interface ($\omega = 90°$), the two exponents degenerate to one real number, governed by the equation

$$\cos(\lambda\pi) = \frac{2(\beta-\alpha)}{(1+\beta)}(1-\lambda)^2 + \frac{\alpha+\beta^2}{1-\beta^2}. \tag{4}$$

Fig. 4 plots the contours of λ on the (α, β) plane. In particular, the contour of $\lambda = 0.5$ is the straight line $\alpha = -\beta$. The crack perpendicularly impinging upon the interface has also been studied by other authors (e.g., Lu and Erdogan, 1983; Chen, 1994; Kang and Lu, 2002; Nuler et al., 2006).

When $\beta = 0$, the exponents are a pair of real numbers, regardless the values of α and ω. Fig. 5 plots the exponents λ_1 and λ_2 as functions of the impinging angle ω, for two values of α. As ω changes from 0 to 90°, the exponents degenerate to 1/2 when the crack lies on the interface, are two unequal numbers when the crack impinges upon the interface at an oblique angle, and degenerate again when the crack is perpendicular to the interface.

Observe that the exponents vary significantly with the elastic mismatch and the impinging angle. As will become evident, the importance of the multiple modes should be assessed on a case-by-case basis.

3. Local mode mixity

In the remainder of this paper, we will focus on the case of two unequal real exponents. As a reference, first recall the best-studied degenerate case: a crack in a homogeneous elastic material, for which the singular stress field is a linear superposition of two modes (e.g., Lawn, 1993):

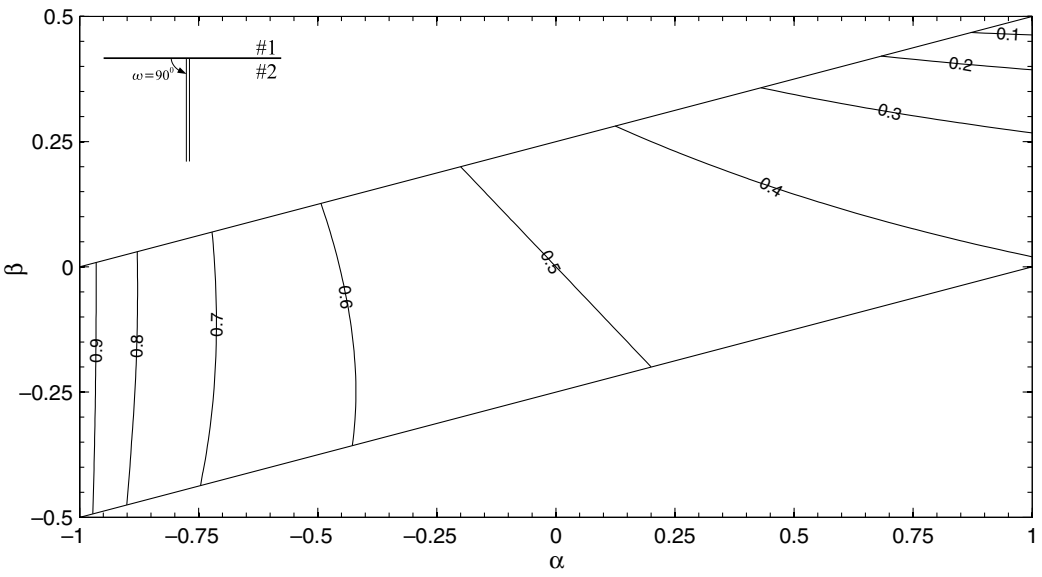

Fig. 4. For a crack impinging perpendicularly on the interface, the two modes of the singular stress field have an identical exponent. Contours of the exponent are plotted on the plane of the Dundurs parameters (α, β).

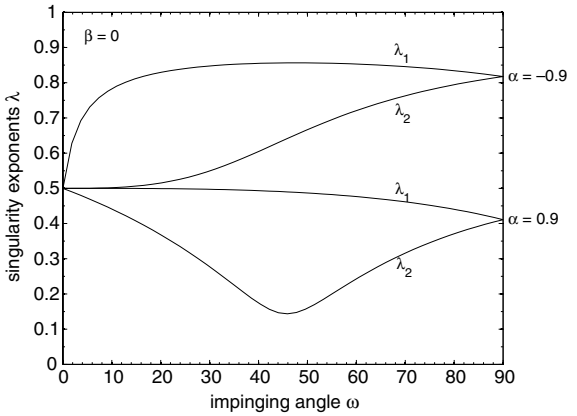

Fig. 5. When $\beta = 0$, and for all values of α and the impinging angle ω, the two modes of the singular stress field are characterized by two real numbers, λ_1 and λ_2. The two exponents are plotted as functions of ω, for $\alpha = 0.9$ and $\alpha = -0.9$. The two exponents degenerate when the crack lies on the interface ($\omega = 0$) and when the crack impinges perpendicularly to the interface ($\omega = 90°$).

$$\sigma_{ij}(r,\theta) = \frac{K_{\mathrm{I}}}{\sqrt{2\pi r}}\Sigma^{\mathrm{I}}_{ij}(\theta) + \frac{K_{\mathrm{II}}}{\sqrt{2\pi r}}\Sigma^{\mathrm{II}}_{ij}(\theta). \tag{5}$$

The plane of the crack is a plane of symmetry, with respect to which the mode I field is symmetric and the mode II field is anti-symmetric. We adopt the conventional normalization: $\Sigma^{\mathrm{I}}_{\theta\theta} = \Sigma^{\mathrm{II}}_{r\theta} = 1$ directly ahead of the crack. The two modes have the same exponents, so that the proportion of the two modes is constant, independent of the distance from the edge of the crack, and can be specified by the ratio of the stress intensity factors, $K_{\mathrm{II}}/K_{\mathrm{I}}$.

For a crack impinging at an oblique angle upon a bimaterial interface (Fig. 1), when the exponents are unequal real numbers λ_1 and λ_2, the singular stress field around the edge of the crack is still a linear superposition of two modes:

$$\sigma_{ij}(r,\theta) = \frac{k_1}{(2\pi r)^{\lambda_1}}\Sigma^1_{ij}(\theta) + \frac{k_2}{(2\pi r)^{\lambda_2}}\Sigma^2_{ij}(\theta). \tag{6}$$

We adopt the normalization that directly ahead of the crack,

$$\Sigma^1_{\theta\theta}(\omega) = 1, \quad \Sigma^2_{r\theta}(\omega) = 1. \tag{7}$$

When the two materials have different elastic constants, however, the plane of the crack is not a plane of symmetry, so that in general $\Sigma^1_{r\theta}(\omega) \neq 0$ and $\Sigma^2_{\theta\theta}(\omega) \neq 0$.

Note that one has to be careful to assess the suitability of the two-mode description (Eq. 6), especially when the second mode is so weak that it may not be much different from the contribution of the non-singular modes. This aspect is not pursued in this paper.

The two stress intensity factors, k_1 and k_2, have different dimensions, being $(\text{stress})(\text{lengh})^{\lambda_1}$ and $(\text{stress})(\text{lengh})^{\lambda_2}$, respectively. Fig. 6 illustrates a representative boundary value problem, with T describing the applied stress, and L the length scale of the macroscopic geometry. Linearity and dimensional considerations dictate that the two stress intensity factors should take the form

$$k_1 = \kappa_1 T L^{\lambda_1}, \quad k_2 = \kappa_2 T L^{\lambda_2}, \tag{8}$$

where κ_1 and κ_2 are dimensionless coefficients.

Eq. (6) suggests that, as the distance r from the edge of the crack varies, the proportion of the two modes also varies and can be specified by the dimensionless parameter $(k_2/k_1)r^{\lambda_1-\lambda_2}$ (Liu et al., 1999). This parameter is suitable to describe the mode mixity of the singular stress field, so long as an arbitrary length r is chosen, in the same spirit as Rice (1988) suggestion for a crack lying on a bimaterial interface. Indeed, Labossiere et al. (2002) have used this mode mixity in describing their experimental data.

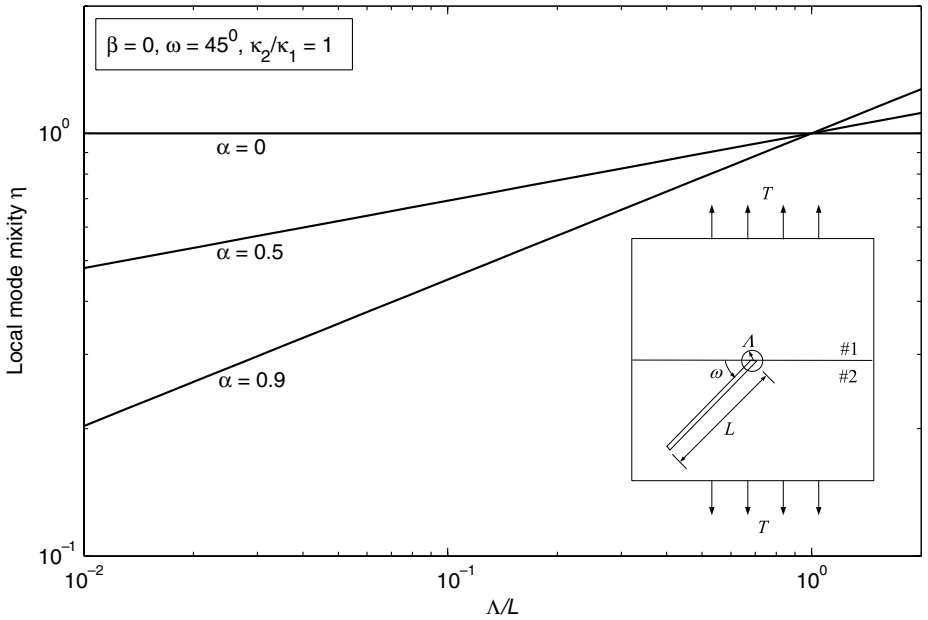

Fig. 6. The inset illustrates a representative boundary value problem, with a macroscopic length L, an applied stress T, and a microscopic length Λ that characterizes the size of a zone in which processes of fracture occur. The proportion of the two modes of the singular stress field at length scale Λ is characterized by the local mode mixity, $\eta = (\kappa_2/\kappa_1)(\Lambda/L)^{\lambda_1-\lambda_2}$; see the body of the paper for interpretation. The parameter η is plotted as a function of Λ/L for three values of α.

The singular stress field (6) is obtained by assuming that the materials are elastic, and the geometry is perfect (Fig. 1). Such assumptions are invalid in a process zone around the edge of the crack, either because the materials deforms plastically, or because the geometry is imperfect. Let Λ be the size of the process zone, within which the singular stress field (6) is invalid. Also, the singular stress field (6) is invalid at size scale L, where the external boundary conditions will change the stress distribution. However, provided the process zone is significantly smaller than the macroscopic length, $\Lambda \ll L$, the singular stress field (6) prevails within an annulus, known as the k-annulus, of some radii bounded between Λ and L.

The microscopic processes of fracture occur within the process zone, but are driven by the singular stress field in the k-annulus. In discussing the effect of the mode mixity on failure processes, it is intuitive to select the length characterizing the size of the process zone, i.e., setting $r = \Lambda$. Thus, we specify a dimensionless parameter

$$\eta = (k_2/k_1)\Lambda^{\lambda_1-\lambda_2} = (\kappa_2/\kappa_1)(\Lambda/L)^{\lambda_1-\lambda_2}. \tag{9}$$

This parameter, to be called the *local mode mixity*, measures the relative contribution of the two modes to the stress field at length scale Λ. The parameter η combines the effects of the loading mixity κ_2/κ_1, the length ratio Λ/L, and the difference of the two exponents λ_1 and λ_2.

As an illustration, consider a loading condition that $\kappa_2/\kappa_1 = 1$, so that the local mode mixity reduces to $\eta = (\Lambda/L)^{\lambda_1-\lambda_2}$, which is plotted in Fig. 6 for the case $\omega = 45°$ and $\beta = 0$. When the elastic mismatch is small (e.g., $\alpha = 0$), the two modes make comparable contributions for all values of Λ/L. When the elastic mismatch is modest (e.g., $\alpha = 0.5$), the two modes make comparable contributions if Λ/L is modest, but the weaker singularity makes a smaller contribution if $\Lambda/L \ll 1$. When the elastic mismatch is large (e.g., $\alpha = 0.9$), the weaker singularity makes negligible contribution so long as Λ is reasonably small compared to L.

As another example, consider a well-bonded interface of two brittle materials, e.g., a thin film epitaxially grown on a substrate. The process zone is taken to be some multiple of atomic dimension, say $\Lambda = 1$ nm. Take L as the thickness of a film, say $L = 100$ nm. For a modest elastic mismatch, we may take $\lambda_1 - \lambda_2 = 0.2$ and $(\Lambda/L)^{\lambda_1-\lambda_2} = 0.4$. Consequently, a modest value of κ_2/κ_1 will bring the local mode mixity η to the order of unity.

4. The competition between penetration and debond

We now analyze the effects of the split singularities on the penetrating and debonding cracks. For simplicity, we will take $\beta = 0$, so that the singular stress field for the crack impinging upon the interface is a superposition of two modes of unequal real exponents, Eq. (6), with the stress intensity factors k_1 and k_2 given by (8). The length Λ now is identified with the length a of the small cracks in Fig. 2, so that the local mode mixity is defined as $\eta = (\kappa_2/\kappa_1)(a/L)^{\lambda_1-\lambda_2}$.

4.1. Penetration

Consider the case that the impinging crack penetrates across the interface (Fig. 2a). The size of the penetrating crack, a, is taken to be small compared to the macroscopic length scale L. The stress field around the edge of the penetrating crack is square-root singular, with the regular stress intensity factors $K_{\mathrm{I}}^{\mathrm{p}}$ and $K_{\mathrm{II}}^{\mathrm{p}}$. At a distance much larger than a, in the k-annulus, the singular stress field (6) prevails, with the stress intensity factors k_1 and k_2. Linearity and dimensional considerations relate the two sets of the stress intensity factors, $(K_{\mathrm{I}}^{\mathrm{p}}, K_{\mathrm{II}}^{\mathrm{p}})$ and (k_1, k_2), as

$$\frac{K_{\mathrm{I}}^{\mathrm{p}}}{\sqrt{a}} = b_{11}\cdot\frac{k_1}{a^{\lambda_1}} + b_{12}\cdot\frac{k_2}{a^{\lambda_2}}, \tag{10}$$

$$\frac{K_{\mathrm{II}}^{\mathrm{p}}}{\sqrt{a}} = b_{21}\cdot\frac{k_1}{a^{\lambda_1}} + b_{22}\cdot\frac{k_2}{a^{\lambda_2}}. \tag{11}$$

The coefficients b_{11}, b_{12}, b_{21} and b_{22} are dimensionless functions of the Dundurs parameter α, the impinging angle ω, and the penetrating angle ϕ. These coefficients are calculated using the finite element method (Appendix), and are listed in Table 1.

Taking the ratio of (11) and (10), we obtain the mode angle of the penetrating crack, ψ^{p}, given by

$$\tan\psi^{\mathrm{p}} = \frac{K_{\mathrm{II}}^{\mathrm{p}}}{K_{\mathrm{I}}^{\mathrm{p}}} = \frac{b_{21}+b_{22}\eta}{b_{11}+b_{12}\eta}. \tag{12}$$

Table 1
Coefficients b_{11}, b_{12}, b_{21}, b_{22} in the range of $5^\circ \leqslant \phi \leqslant 170^\circ$ for $\alpha = -0.5$, 0, and 0.5 with $\beta = 0$ and $\omega = 45^\circ$

ϕ (°)	α											
	−0.5	0	0.5	−0.5	0	0.5	−0.5	0	0.5	−0.5	0	0.5
	b_{11}			b_{12}			b_{21}			b_{22}		
5	−0.640	0.840	1.418	3.525	0.921	1.098	−1.268	−0.291	−0.007	−0.798	0.652	0.886
10	−0.486	0.876	1.412	3.617	0.831	0.954	−1.359	−0.264	0.054	−0.642	0.728	0.970
20	−0.153	0.935	1.381	3.737	0.624	0.631	−1.488	−0.199	0.159	−0.282	0.856	1.121
30	0.205	0.978	1.322	3.759	0.387	0.269	−1.548	−0.124	0.252	0.114	0.948	1.221
40	0.568	0.999	1.240	3.679	0.131	−0.112	−1.537	−0.042	0.331	0.517	0.995	1.258
45	0.747	1.002	1.191	3.601	0.000	−0.302	−1.506	0.000	0.364	0.712	1.002	1.252
50	0.920	0.999	1.138	3.498	−0.131	−0.490	−1.458	0.042	0.393	0.900	0.996	1.229
60	1.246	0.978	1.022	3.224	−0.387	−0.848	−1.314	0.124	0.438	1.240	0.949	1.137
70	1.530	0.935	0.897	2.874	−0.625	−1.166	−1.115	0.199	0.465	1.516	0.859	0.989
80	1.761	0.876	0.769	2.466	−0.832	−1.430	−0.873	0.264	0.474	1.713	0.731	0.798
90	1.931	0.801	0.642	2.022	−1.003	−1.630	−0.600	0.315	0.466	1.823	0.574	0.578
100	2.035	0.715	0.519	1.565	−1.128	−1.761	−0.311	0.350	0.442	1.844	0.399	0.345
110	2.072	0.623	0.406	1.121	−1.206	−1.821	−0.024	0.369	0.406	1.780	0.217	0.119
120	2.044	0.528	0.303	0.707	−1.236	−1.815	0.251	0.371	0.360	1.642	0.039	−0.089
130	1.957	0.435	0.213	0.338	−1.221	−1.750	0.501	0.358	0.307	1.445	−0.124	−0.263
140	1.818	0.347	0.137	0.028	−1.165	−1.638	0.715	0.331	0.250	1.209	−0.264	−0.392
150	1.630	0.266	0.076	−0.222	−1.075	−1.491	0.889	0.294	0.190	0.947	−0.375	−0.470
160	1.411	0.197	0.030	−0.405	−0.960	−1.327	1.015	0.250	0.133	0.690	−0.449	−0.491
170	1.161	0.138	−0.002	−0.531	−0.828	−1.157	1.090	0.202	0.080	0.446	−0.486	−0.461

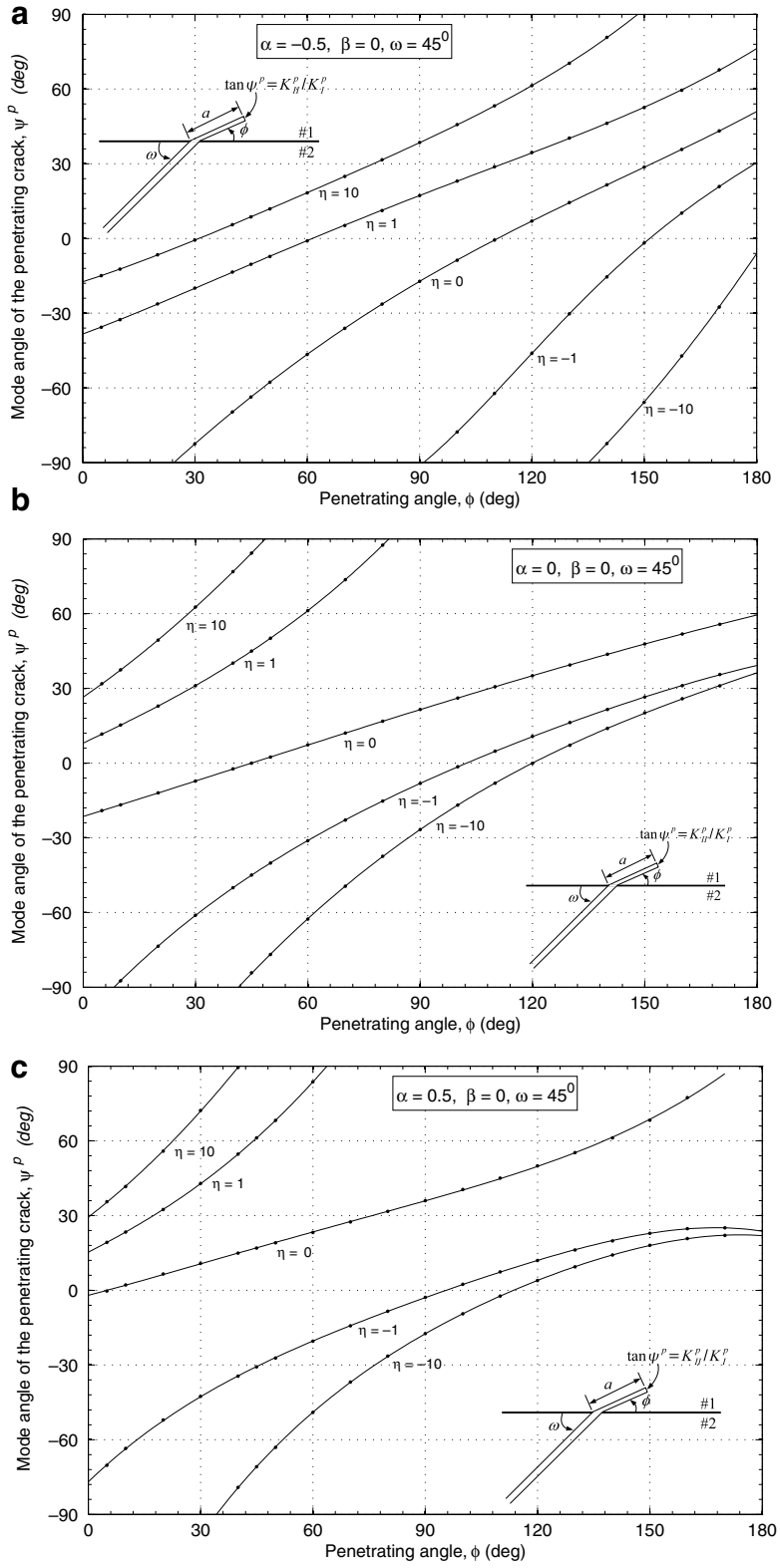

Fig. 7. Mode angle of a penetrating crack, ψ^{p}, is plotted as a function of the penetrating angle ϕ, for several values of the local mode mixity η. The dots on the curves are the results of finite element calculation. (a) $\alpha = -0.5$, (b) $\alpha = 0$, and (c) $\alpha = +0.5$.

Fig. 7 plots the mode angle ψ^{p} as a function of the penetrating angle, ϕ, for some values of η and α, with $\beta = 0$ and $\omega = 45°$. We require that $K_{\mathrm{I}}^{\mathrm{p}} > 0$, i.e., $k_1 a^{1/2-\lambda_1}(b_{11} + b_{12}\cdot\eta) > 0$. When the two materials have dissimilar elastic constants, k_1 no longer stands for the stress intensity factor of opening mode, so it may be either positive or negative. In this paper, we adopt $k_1 > 0$ for the presentation of the results.

If the toughness of material #1 is anisotropic, a cleavage plane may set the penetrating angle ϕ. If the toughness of material #1 is isotropic, however, the penetrating angle ϕ may be selected by requiring that the penetrating crack be purely mode I, namely, $K_{\mathrm{II}}^{\mathrm{p}} = 0$. Such a penetrating angle, denoted by ϕ^*, corresponds to the intersection of a curve in Fig. 7 with the horizontal line $\psi^{\mathrm{p}} = 0$. For example, if the contribution of k_2 is neglected, i.e., $\eta = 0$, the impinging crack prefers to deflect onto the interface when $\alpha \geqslant 0.5$ (Fig. 7c), as stated in He and Hutchinson (1989a). When k_2 is included, however, the crack may penetrate across the interface.

Fig. 8 plots penetrating angle ϕ^* as a function of the local mode mixity η. For the curve that the two materials have the same elastic constants, our results match well with those of Hayashi and Nemat-Nasser (1981) and He and Hutchinson (1988, 1989b). When $\eta = 0$, the impinging crack is under mode I loading and penetrates straight ahead, $\phi^* = 45°$. When, $\eta > 0$ the impinging crack is under a mixed mode condition and may penetrate across the interface at an angle $\phi^* < 45°$. When $\eta > 0.545$, however, ϕ^* becomes negative, so that the impinging crack can no longer penetrate across the interface. This feature is also observed for the case of $\alpha = 0.5$, where ϕ^* becomes negative when $\eta > 0.05$.

4.2. Debond

We next consider the case that the impinging crack causes the interface to debond (Fig. 2b). When $\beta = 0$, the stress field at the edge of the interfacial crack is square-root singular, with the regular stress intensity factors, $(K_{\mathrm{I}}^{\mathrm{d}}, K_{\mathrm{II}}^{\mathrm{d}})$. They relate to the stress intensity factors of the impinging crack (k_1, k_2) as

$$\frac{K_{\mathrm{I}}^{\mathrm{d}}}{\sqrt{a}} = c_{11}\cdot\frac{k_1}{a^{\lambda_1}} + c_{12}\cdot\frac{k_2}{a^{\lambda_2}}, \tag{13}$$

$$\frac{K_{\mathrm{II}}^{\mathrm{d}}}{\sqrt{a}} = c_{21}\cdot\frac{k_1}{a^{\lambda_1}} + c_{22}\cdot\frac{k_2}{a^{\lambda_2}}. \tag{14}$$

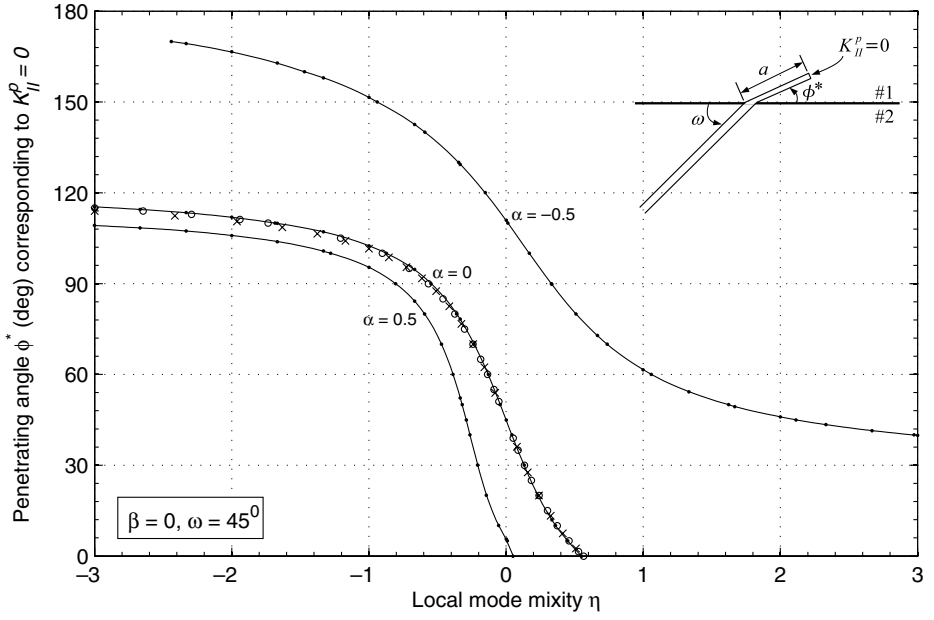

Fig. 8. Penetrating angle ϕ^* corresponding to $K_{\mathrm{II}}^{\mathrm{p}} = 0$ is plotted as a function of the local mode mixity η. For the case of $\alpha = 0$, the results by Hayashi and Nemat-Nasser (1981) are marked by crosses, and those by He and Hutchinson (1988, 1989b) by open circles.

The dimensionless parameters c_{11}, c_{12}, c_{21} and c_{22} are functions of α and ω. The results calculated using the finite element method are listed in Table 2. For the case of $\alpha = 0$, we can compare our results with those of He and Hutchinson (1988), and the difference is within 2%.

Taking the ratio of (14) and (13), we obtain the mode angle of the debonding crack, ψ^{d}, as given by

$$\tan\psi^{\mathrm{d}} = \frac{K_{\mathrm{II}}^{\mathrm{d}}}{K_{\mathrm{I}}^{\mathrm{d}}} = \frac{c_{21} + c_{22}\eta}{c_{11} + c_{12}\eta}. \tag{15}$$

Fig. 9 plots the mode angle of the debond crack, ψ^{d} as a function of the local mode mixity η for $\alpha = -0.5$, 0, and 0.5, with $\beta = 0$ and $\omega = 45°$.

4.3. The competition between penetration and debond

For the penetrating crack, the energy release rate relates to the stress intensity factors as (Irwin, 1957)

$$G^{\mathrm{p}} = \frac{(1-\nu_1)}{2\mu_1}[(K_{\mathrm{I}}^{\mathrm{p}})^2 + (K_{\mathrm{II}}^{\mathrm{p}})^2]. \tag{16}$$

For the interfacial crack, the energy release rate relates to the stress intensity factors as (Malyshev and Salganik, 1965)

$$G^{\mathrm{d}} = \left(\frac{1-\nu_1}{4\mu_1} + \frac{1-\nu_2}{4\mu_2}\right)[(K_{\mathrm{I}}^{\mathrm{d}})^2 + (K_{\mathrm{II}}^{\mathrm{d}})^2]. \tag{17}$$

Table 2
Coefficients c_{11}, c_{12}, c_{21} and c_{22} for different α with $\beta = 0$ and $\omega = 45°$

α	−0.5	0	0.5
c_{11}	−0.859	0.801	0.989
c_{12}	4.248	0.999	0.924
c_{21}	−1.466	−0.315	−0.166
c_{22}	−0.852	0.571	0.493

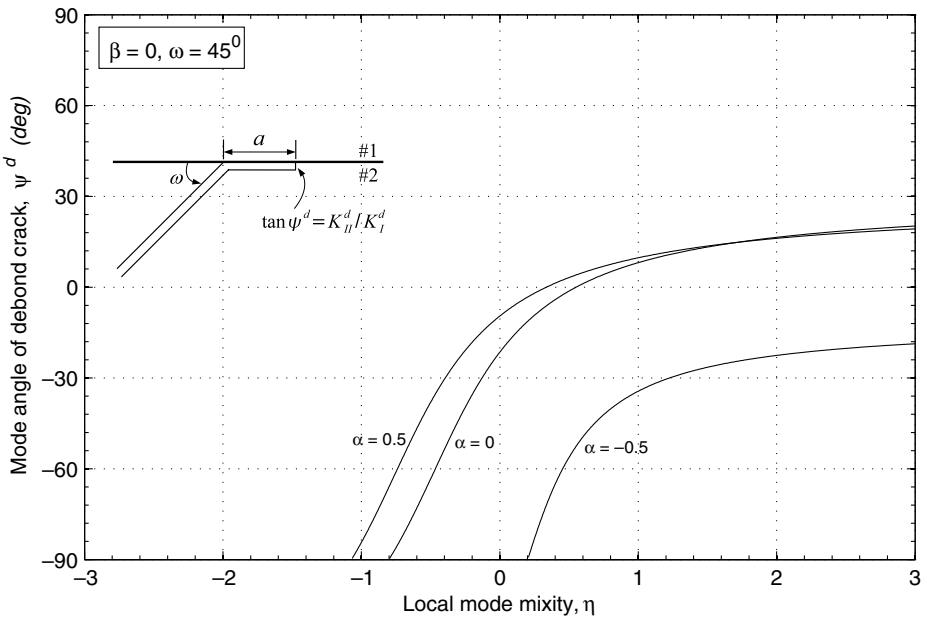

Fig. 9. Mode angle of the debond crack, ψ^{d}, is plotted as a function of local mode mixity η.

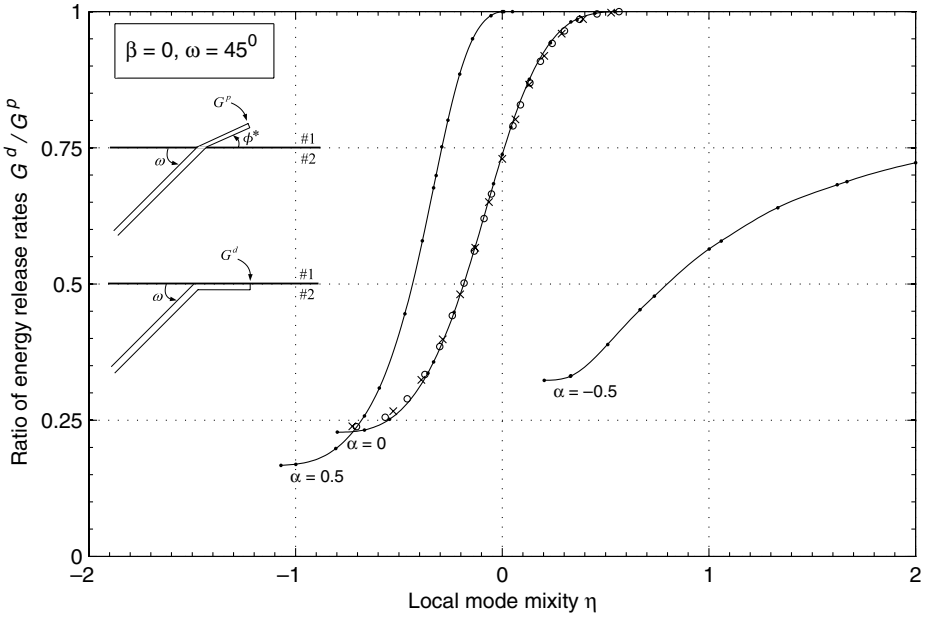

Fig. 10. Ratio of the energy release rate of the debond crack, G^{d}, to the energy release rate of the penetration crack, G^{p}, is plotted as a function of the local mode mixity η. For the case of $\alpha = 0$, the results by Hayashi and Nemat-Nasser (1981) are marked by crosses, and those by He and Hutchinson (1988, 1989b) by open circles.

The ratio of the energy release rate of the debonding crack to that of the penetrating crack is

$$\frac{G^{\mathrm{d}}}{G^{\mathrm{p}}} = \frac{1}{1-\alpha}\cdot\frac{(c_{11}^2+c_{21}^2)+2(c_{11}c_{12}+c_{21}c_{22})\eta+(c_{12}^2+c_{22}^2)\eta^2}{(b_{11}^2+b_{21}^2)+2(b_{11}b_{12}+b_{21}b_{22})\eta+(b_{12}^2+b_{22}^2)\eta^2}. \tag{18}$$

Here we have assumed that the sizes of flaws in material #1 and on the interface take the same value a. The mode angle of the penetration crack is selected by requiring $K_{\mathrm{II}}^{\mathrm{p}} = 0$, as discussed above. Fig. 10 plots the ratio $G^{\mathrm{d}}/G^{\mathrm{p}}$ as a function of η for $\alpha = -0.5$, 0, and 0.5 with $\beta = 0$ and $\omega = 45°$. For each value of α, the curve is limited in an interval of η to ensure that both the penetrating crack and the debonding crack are open, i.e., $K_{\mathrm{I}}^{\mathrm{p}} > 0$ and $K_{\mathrm{I}}^{\mathrm{d}} > 0$. For the case $\alpha = 0$, we have confirmed our results with those of Hayashi and Nemat-Nasser (1981) and He and Hutchinson (1988, 1989b).

Let Γ_1 be the fracture energy of material #1 under the mode I condition, and Γ_{i} be the fracture energy of the interface at the mode angle ψ^{d}. If $\Gamma_{\mathrm{i}}/\Gamma_1 > G^{\mathrm{d}}/G^{\mathrm{p}}$, the impinging crack will penetrate across the interface, rather than debond the interface. Otherwise, the impinging crack will debond the interface, rather than penetrate across the interface.

5. Discussions

5.1. Will the weaker singularity affect the competition between penetration and debond?

The relative magnitude of the two modes of singularities is characterized by the local mode mixity $\eta = (\kappa_2/\kappa_1)(a/L)^{\lambda_1-\lambda_2}$. Thus, the effect of the weaker singularity on the penetration–debond competition will depend on how sensitive the competition depends on η, and on how large η is. We next address these two questions.

The local mode mixity η affects the penetration–debond competition in two ways. First, η affects the mode angle of the debonding crack (Fig. 9). The mode angle, in its turn, affects the fracture energy of the interface (e.g., Hutchinson and Suo, 1992). Second, η affects the ratio $G^{\mathrm{d}}/G^{\mathrm{p}}$, Fig. 10. Consequently, the weaker singu-

larity may readily alter the outcome of the penetration–debond competition, provided the local mode mixity η is not too small.

The value of η will depend on the ratio κ_2/κ_1, which in turn depends on the external geometry and loads. In practice, the ratio κ_2/κ_1 can be anywhere from $-\infty$ to ∞. When the elastic constants of the two materials are not too different, the two exponents will be nearly the same, so that $(a/L)^{\lambda_1-\lambda_2} \approx (a/L)^0 = 1$, and the local mode mixity reduces to the mode mixity for a crack in a homogeneous material, $\eta = \kappa_2/\kappa_1$. When the elastic constants of the two materials are very different, however, the local mode mixity will vary with a/L, as illustrated in Fig. 6. If a is much smaller than L, so that $\eta \ll 1$, then the weaker singularity should have little effect on the penetration–debond competition, in which case the value of a is irrelevant. On the other hand, if η is large, then the value of a influences the outcome of the competition. In this case, because the flaw size is statistical, we expect that the outcome of the competition is also statistical.

5.2. Alternative models and interpretations of Λ

Following He and Hutchinson (1989a), we have assumed that (i) small cracks, of some length a, pre-exists on the interface and in material #1, and (ii) the materials are elastic to the scale somewhat below a, so that fracture mechanics can be applied to the small cracks. These assumptions may not be valid in applications. For example, the material and the bonding may be of such a high quality that no small cracks are present in the zone of influence of the impinging crack. In such a case, if the materials are elastic to some size scale, we may directly use the stress field Eq. (6) to estimate the stresses just outside the inelastic zone. Thus, the parameter $\eta = (\kappa_2/\kappa_1)(\Lambda/L)^{\lambda_1-\lambda_2}$ still characterizes the mode mixity at the length scale of the inelastic zone, but with Λ interpreted as the size of the inelastic zone. To determine whether the crack will penetrate across, or debond, the interface, the ratio of the strength of the interface and the strength of the material may be compared with the ratio of the corresponding stresses predicted from Eq. (6) at distance $r = \Lambda$. Such a stress-based model has long been used (e.g., Cook and Gordon, 1964; Gupta et al., 1992), and can be extended to include the effect of the split singularities.

As another example, the inelastic zone may be large compared to the small cracks, but still small compared to the macroscopic length L. In such a case, one may include inelastic process explicitly in the model. One approach is to use cohesive laws to represent the fracture process in materials and on the interface (Mohammed and Liechti, 2000; Parmigiani and Thouless, 2006). In such a model, Λ may be identified as $\Lambda = E\Gamma/S^2$, where E is Young's modulus of a material, Γ the fracture energy, and S the theoretical strength. Even in such a case, the notion of split singularities is still important, as they set the mode mixity at the relevant length scale.

5.3. The size of the flaw on the interface may be different from that in the material

In reaching Eq. (18), we have assumed that the flaws on the interface and in material #1 have an equal size. In reality, these flaws may have different sizes, say, a^{d} and a^{p}, respectively. Consequently, Eqs. (16) and (17) leads to

$$\frac{G^{\mathrm{d}}}{G^{\mathrm{p}}} = \frac{1}{1-\alpha}\cdot\frac{(c_{11}^2+c_{21}^2)+2(c_{11}c_{12}+c_{21}c_{22})\eta^{\mathrm{d}}+(c_{12}^2+c_{22}^2)(\eta^{\mathrm{d}})^2}{(b_{11}^2+b_{21}^2)+2(b_{11}b_{12}+b_{21}b_{22})\eta^{\mathrm{p}}+(b_{12}^2+b_{22}^2)(\eta^{\mathrm{p}})^2}\left(\frac{a^{\mathrm{d}}}{a^{\mathrm{p}}}\right)^{1-2\lambda_1}. \tag{19}$$

If the elastic mismatch of the two materials is not extremely large, λ_1 will be not too far from 1/2 and the difference in λ_1 and λ_2 is not too large; see Figs. 3–5. Consequently, for a modest difference in a^{d} and a^{p}, $(a^{\mathrm{d}}/a^{\mathrm{p}})^{1-2\lambda_1} \approx 1$ and $\eta^{\mathrm{d}}/\eta^{\mathrm{p}} = (a^{\mathrm{d}}/a^{\mathrm{p}})^{\lambda_1-\lambda_2} \approx 1$, so that (19) reduces to (18). On the other hand, when the elastic mismatch or the difference in a^{d} and a^{p} is large, one should use Eq. (19) instead of (18). In this case, because the flaw sizes are usually unknown, the outcome of penetration–debond competition should be statistical.

6. Concluding remarks

The singular stress field around the edge of a crack impinging on a bimaterial interface is a linear superposition of two modes, often of unequal exponents, λ_1 and λ_2. So long as the process zone size Λ is small com-

pared with the macroscopic length L, the singular field prevails in an annulus of some radii bounded between Λ and L. We characterize the proportion of the two modes at the size scale Λ by a dimensionless parameter, $\eta = (\kappa_2/\kappa_1)(\Lambda/L)^{\lambda_1-\lambda_2}$, called the local mode mixity. We show that the weaker singularity may readily affect whether the crack will penetrate across, or debond, the interface. Because the split singularities occur in many configurations of cracks and wedges, the approach outlined in this paper may find broad applications.

Acknowledgements

The results reported here were obtained in the course of research funded by Intel Corporation through a contract from the Semiconductor Research Corporation.

Appendix A. Determination of coefficients b_{11}, b_{12}, b_{21}, b_{22}, c_{11}, c_{12}, c_{21} and c_{22}

We solve four boundary value problems sketched in Figs. A.1 and A.2, using the finite element code ABAQUS 6.5. Plane strain conditions are assumed, and Poisson's ratios of both materials are set to be 0.5, so that $\beta = 0$. The stress intensity factors of the primary crack, k_1 and k_2, are obtained by fitting Eq. (6) with the stresses calculated for problems in Fig. A.1, along $\theta = \omega$ within $10^{-3} < r/R < 10^{-2}$. For the problems in Fig. A.2, the size of the penetrating crack a is set to be $R/1000$. The stress intensity factors of the penetrating crack, $K_{\mathrm{I}}^{\mathrm{p}}$, $K_{\mathrm{II}}^{\mathrm{p}}$, are read from the outputs of contour integrals. These stress intensity factors, along with the linear relations (10) and (11), allow us to solve the coefficients b_{11}, b_{12}, b_{21} and b_{22}. Similarly, we use the finite

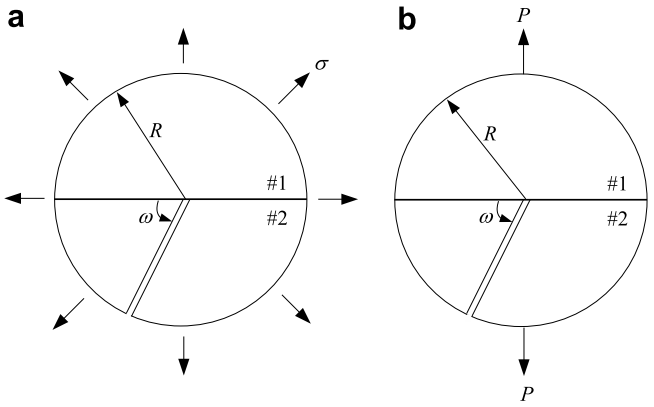

Fig. A.1. The geometry and loading conditions for the primary crack. (a) Biaxial tension. (b) Stretch by a pair of forces.

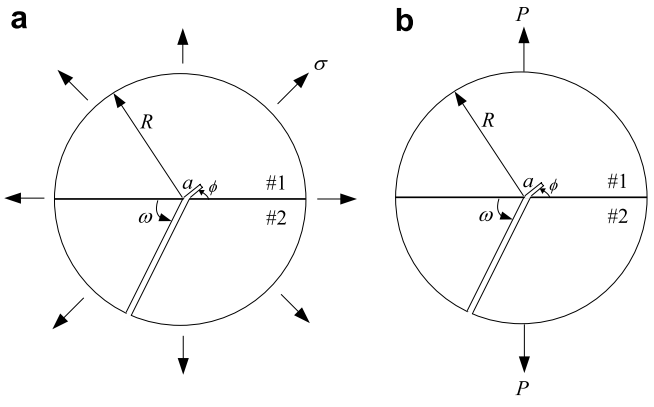

Fig. A.2. The two loading cases for the primary crack to penetrate across the interface. (a) Biaxial tension. (b) Stretch by a pair of forces.

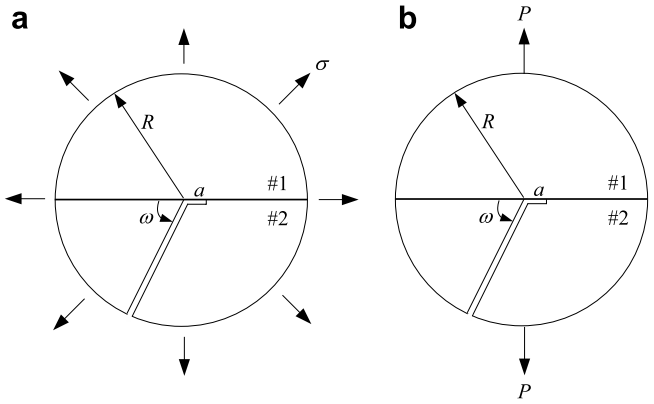

Fig. A.3. The two loading cases for the primary crack to deflect and debond the interface. (a) Biaxial tension. (b) Stretch by a pair of forces.

element code to solve the boundary value problems in Figs. A.1 and A.3, which allow us to determine the coefficients c_{11}, c_{12}, $c_{21}$and c_{22} in (13) and (14).

References

Akisanya, A.R., Fleck, N.A., 1997. Interfacial cracking from the free-edge of a long bi-material strip. Int. J. Solids Struct. 34, 1645–1665.

Ashaugh, N.E., 1975. Stress solution for a crack at an arbitrary angle to an interface. Int. J. Fract. 11, 205–219.

Bogy, D.B., 1971. On the plane elastostatic problem of a loaded crack terminating at a material interface. J. Appl. Mech. 38, 911–918.

Chen, D.H., 1994. A crack normal to and terminating at a bimaterial interface. Eng. Fract. Mech. 49 (4), 517–532.

Chen, J.-T., Wang, W.-C., 1996. Experimental analysis of an arbitrarily inclined semi-infinite crack terminated at the bi-material interface. Exp. Mech. 36 (1), 7–16.

Cook, J., Gordon, J.E., 1964. A mechanism for the control of crack propagation in all-brittle systems. Proc. R. Soc. London A 282 (139), 508–520.

Davis, J.B., Kristoffersson, A., Carlstrom, E., Clegg, W.J., 2000. Fabrication and crack deflection in ceramic laminates with porous interlayers. J. Am. Ceram. Soc. 83 (10), 2369–2374.

Dundurs, J., 1969. Edge-bonded dissimilar orthogonal elastic wedges. J. Appl. Mech. 36, 650–652.

Dunn, M.L., Hui, C.Y., Labossiere, P.E.W., Lin, Y.Y., 2001. Small scale geometric and material features at geometric discontinuities and their role in fracture analysis. Int. J. Fract. 110, 101–121.

Fenner, D.N., 1976. Stress singularities in composite materials and an arbitrary oriented crack meeting an interface. Int. J. Fract. 12, 705–721.

Gupta, V., Argon, A.S., Suo, Z., 1992. Crack deflection at an interface between two orthotropic media. J. Appl. Mech. 59, S79–S87.

Hayashi, K., Nemat-Nasser, S., 1981. Energy-release rate and crack kinking under combined loading. J. Appl. Mech. 48, 520–524.

He, M-Y., Hutchinson, J.W., 1988. Kinking of a crack out of an interface: tabulated solution coefficients. Harvard University Report MECH-113A.

He, M.-Y., Hutchinson, J.W., 1989a. Crack deflection at an interface between dissimilar elastic materials. Int. J. Solids Struct. 25 (9), 1053–1067.

He, M.-Y., Hutchinson, J.W., 1989b. Kinking of a crack out of an interface. J. Appl. Mech. 56, 270–278.

Hui, C.Y., Ruina, A., 1995. Why K? High order singularities and small scale yielding. Int. J. Fract. 72, 97–120.

Hutchinson, J.W., Suo, Z., 1992. Mixed mode cracking in layered materials. Adv. Appl. Mech. 29, 63–191.

Irwin, G.R., 1957. Analysis of stresses and strains near the end of a crack traversing a plate. J. Appl. Mech. 24, 361–364.

Joyce, M.R., Reed, P.A.S., Syngellakis, S., 2003. Numerical modeling of crack shielding and deflection in a multi-layered material system. Mater. Sci. Eng. A 342, 11–22.

Kang, Y., Lu, H., 2002. Investigation of near-tip displacement fields of a crack normal to and terminating at a bimaterial interface under mixed-mode loading. Eng. Fract. Mech. 69, 2199–2208.

Kovar, D., Thouless, M.D., Halloran, J.W., 1998. Crack deflection and propagation in layered silicon nitride/boron nitride ceramics. J. Am. Ceram. Soc. 81 (4), 1004–1012.

Labossiere, P.E.W., Dunn, M.L., Cunningham, S.J., 2002. Application of bimaterial interface corner failure mechanics to silicon/glass anodic bonds. J. Mech. Phys. Solids 50, 405–433.

Lawn, B., 1993. Fracture of Brittle Solids, second ed. Cambridge University Press.

Leguillon, D., Lacroix, C., Martin, E., 2000. Interface debonding ahead of a primary crack. J. Mech. Phys. Solids 48, 2137–2161.

Leguillon, D., Lacroix, C., Martin, E., 2001. Crack deflection by an interface—asymptotics of the residual thermal stress. Int. J. Solids Struct. 38, 7423–7445.

Lemaitre, J., Desmorat, R., Vidonne, M.P., Zhang, P., 1996. Reinitiation of a crack reaching an interface. Int. J. Fract. 80, 257–276.
Li, J., Zhang, X.B., Recho, N., 1997. Investigation of an arbitrarily oriented crack meeting an interface between two elastic materials. Eur. J. Mech. A-Solid. 16 (5), 795–821.
Liu, X.H., Suo, Z., Ma, Q., 1999. Split singularities: stress field near the edge of a silicon die on a polymer substrate. Acta Mater. 47 (1), 67–76.
Lu, M.C., Erdogan, F., 1983. Stress intensity factors in two bonded elastic layers containing cracks perpendicular to and on the interface-I. Anal. Eng. Fract. Mech. 18, 491–506.
Malyshev, B.M., Salganik, R.L., 1965. The strength of adhesive joints using the theory of cracks. Int. J. Fract. Mech. 1 (2), 114–128.
Martinez, D., Gupta, V., 1994. Energy criterion for crack deflection at an interface between two orthotropic media, II: results and experimental verification. J. Mech. Phys. Solids 42, 1247–1271.
Mohammed, I., Liechti, K.M., 2000. Cohesive zone modeling of crack nucleation at bimaterial corners. J. Mech. Phys. Solids 48, 735–764.
Nuler, B., Ryvkin, M., Chudnovsky, A., in press. Crack stability in a vicinity of interface.
Parmigiani, J.P., Thouless, M.D., 2006. The roles of toughness and cohesive strength on crack deflection at interfaces. J. Mech. Phys. Solids 54, 266–287.
Reedy, E.D., 2000. Connection between interface corner and interfacial fracture analyses of an adhesively-bonded butt joint. Int. J. Solids Struct. 37, 2429–2442.
Rice, J.R., 1988. Elastic fracture mechanics concepts for interfacial cracks. J. Appl. Mech. 55, 98–103.
Roham, S., Hardikar, K., Woytowitz, P., 2004. Crack penetration and deflection at a bimaterial interface in a four-point bend test. J. Mater. Res. 19 (10), 3019–3027.
Thouless, M.D., Cao, H.C., Mataga, P.A., 1989. Delamination from surface cracks in composite materials. J. Mater. Sci. 24, 1406–1412.
Williams, M.L., 1959. The stress around a fault or crack in dissimilar media. Bull. Seismol. Soc. Am. 49 (2), 199–204.
Zak, A.R., Williams, M.L., 1963. Crack point singularities at a bi-material interface. J. Appl. Mech. 31, 142–143.